

Figure 1: VAL-1221 degrades LBs *in vitro*. A. Schematic of the VAL-1221 AEF showing the hFab fragment, made of two peptides linked by disulfide bridges, and the GAA enzyme, fused to the hFab heavy chain fragment peptide. B. Reducing and non-reducing SDS-PAGE gel showing the purity of the VAL-1221 construct. Characteristic banding patterns for VAL-1221 are seen. The non-reducing lane shows the full-size VAL-1221 band as well as faint bands indicating unequal production of the two precursor peptides. The reducing lane shows ablation of the full-size band and shows strong bands at the sizes of the precursor peptides. C. *in vitro* activity assay of VAL-1221 using 4-MU-GP as a substrate with 1-, 3-, and 7-day incubations. D. GCMS glucose quantification assay with VAL-1221 on LKO mouse brain homogenate. E. GCMS glucose quantification assay with VAL-1221 on MKO mouse brain homogenate. F. HPAEC-PAD quantification of the molecules released from purified LKO LBs digested with VAL-1221 as a function of time. G. Light microscopy of Lugol's stained purified LKO LBs digested for 168 hours with PBS or VAL-1221. Data presented as mean with standard deviation (SD) error bars, * p≤0.05.

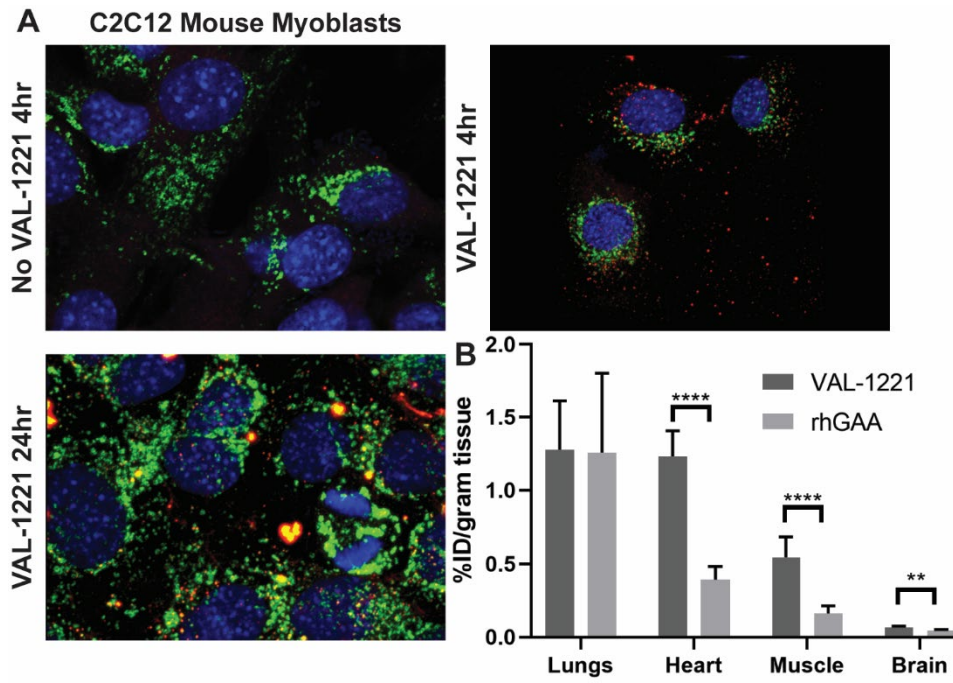


Figure 2: VAL-1221 penetrates cells in culture and distributes to clinically relevant tissues when delivered systemically.
A. Immunofluorescence shows C2C12 Mouse myoblasts take up VAL-1221 into the cytoplasm and lysosomes. Blue: DAPI, Green: LAMP2, Red: VAL-1221. B. Radiolabeled VAL-1221 biodistribution in lungs, heart, quadriceps (muscle), and brain in WT mice after TVI compared to radiolabeled rhGAA. Data presented as mean with SD error bars, ** p≤0.01, **** p≤0.0001.

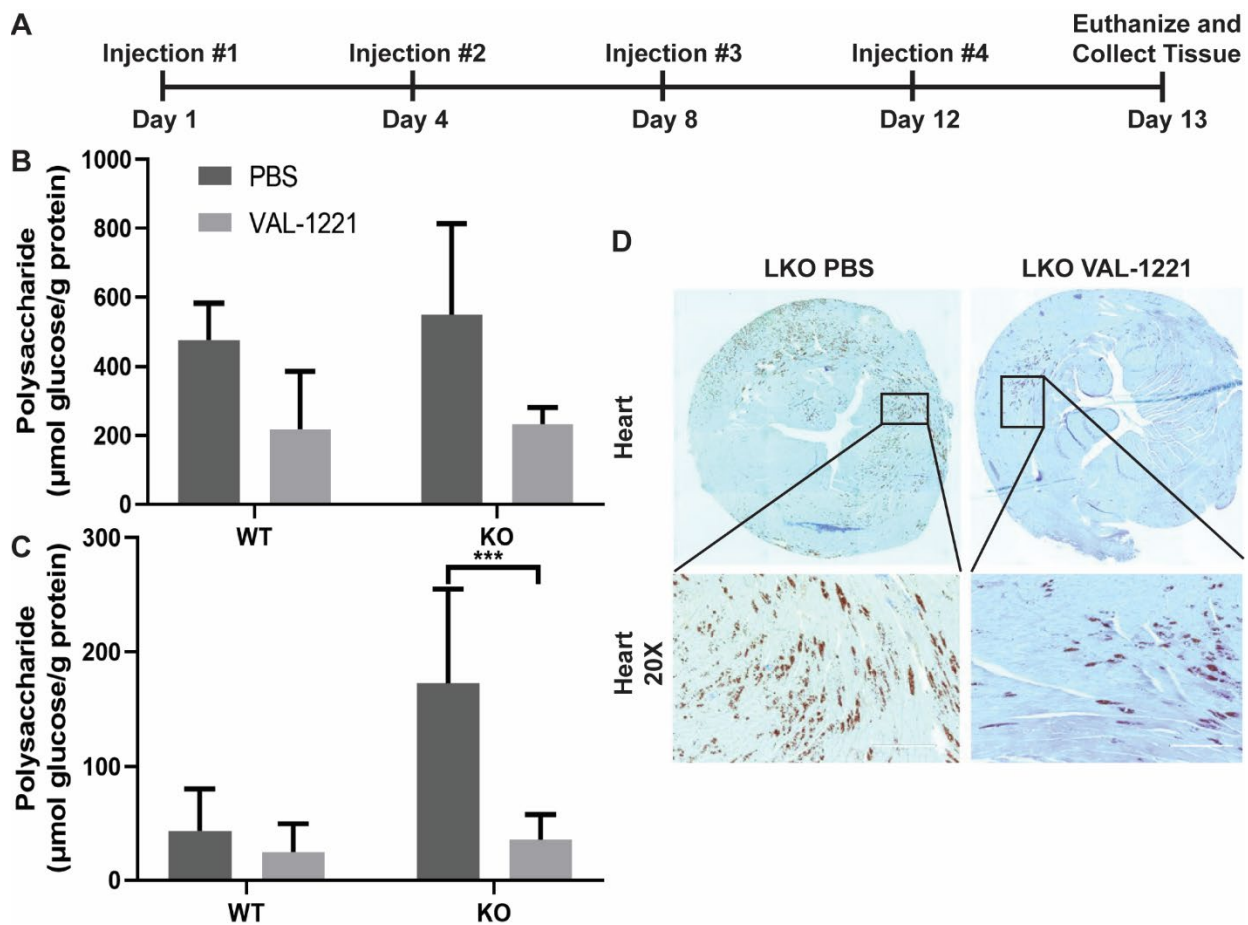
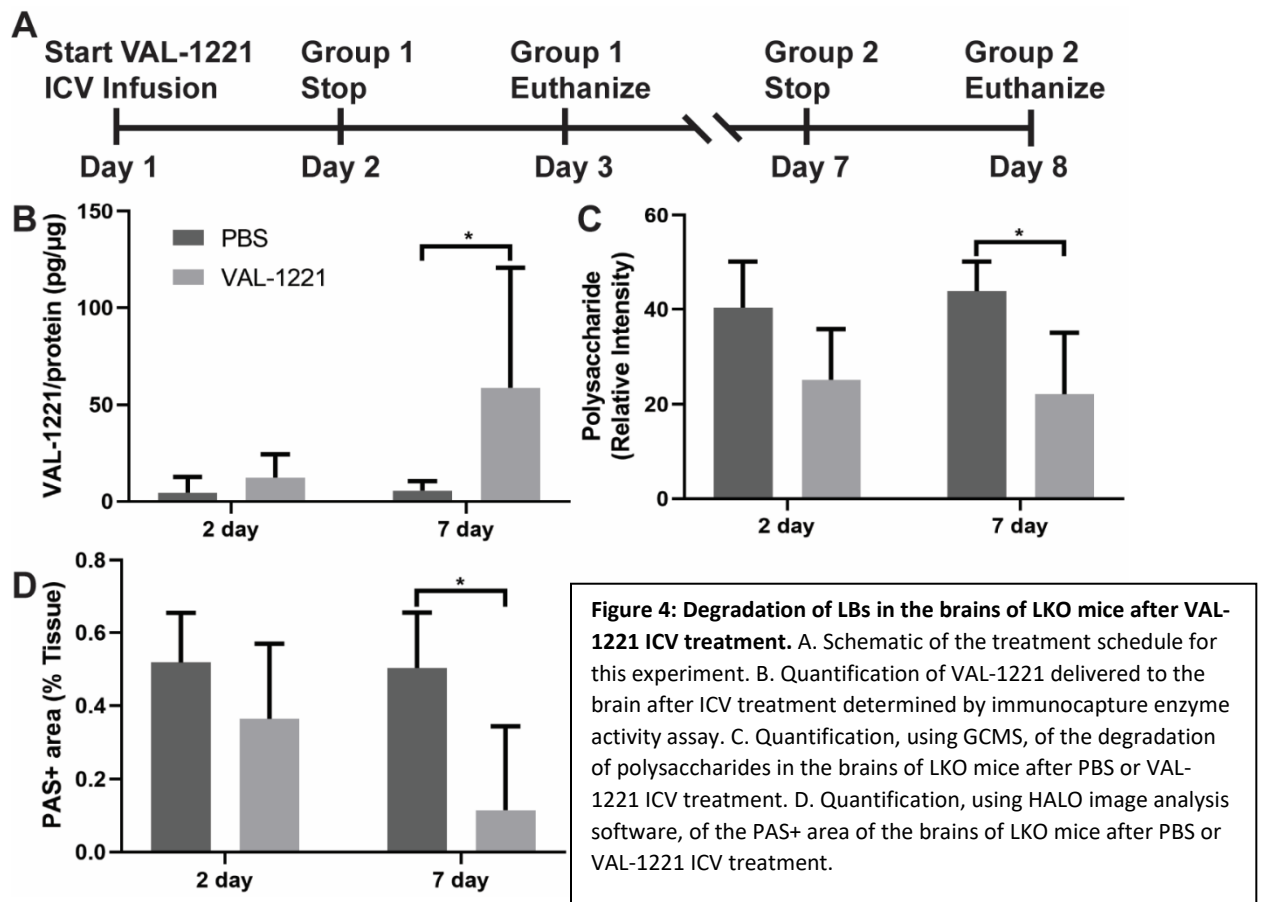


Figure 3: VAL-1221 degrades LBs in heart and quadriceps muscle tissue of LKO mice after TVI. A. Schematic of the injection schedule for this experiment. B. Biochemical quantification of polysaccharides in heart tissue in WT and LKO mice with PBS or VAL-1221 TVI treatment. C. Biochemical quantification of polysaccharides in quadriceps tissue in WT and LKO mice with PBS or VAL-1221 TVI treatment. D. Representative PAS staining of LKO mouse heart tissue after TVI treatment with PBS or VAL-1221. Data presented as mean with SD error bars, *** $p \leq 0.001$.



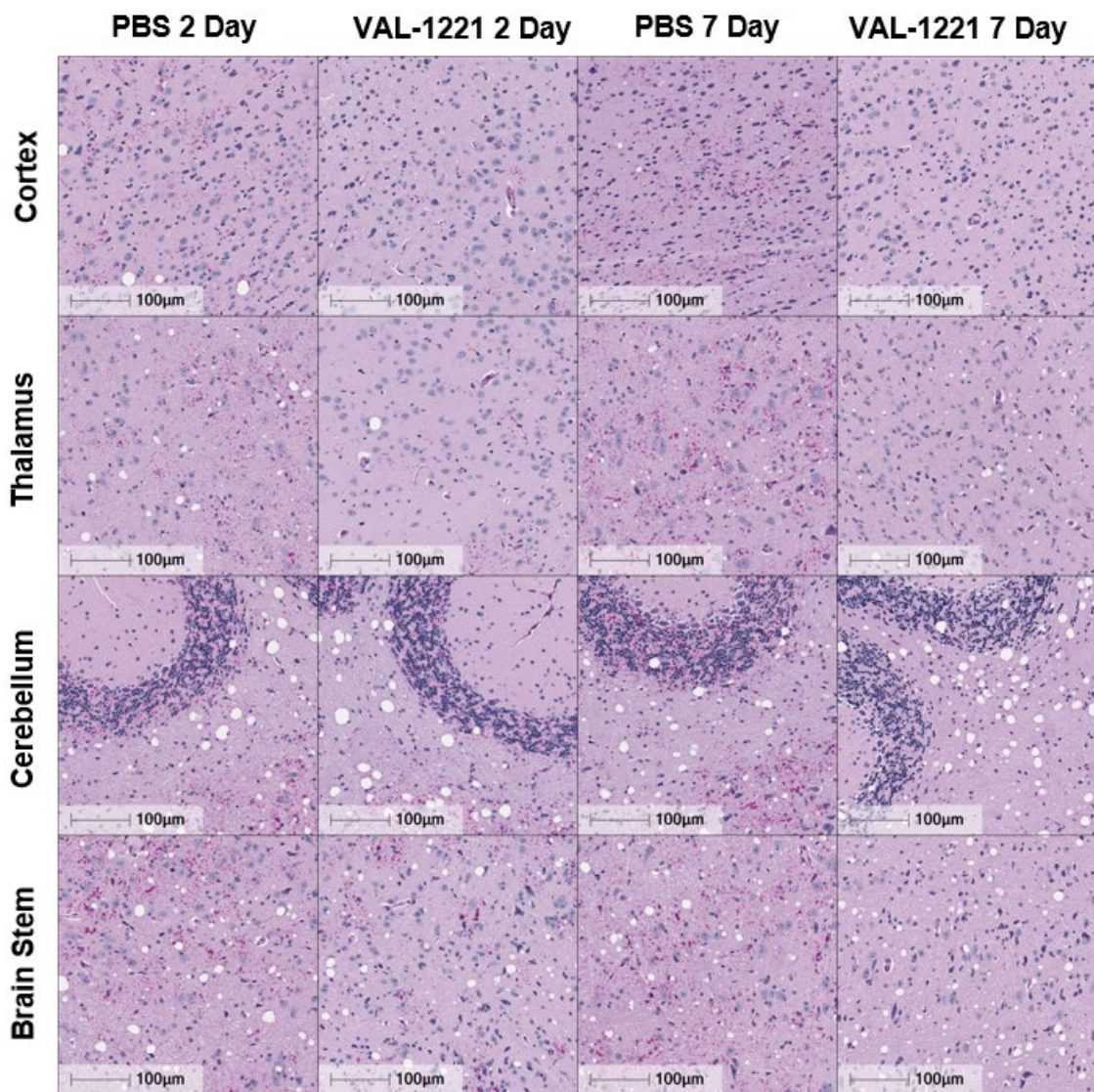


Figure 5: PAS staining of brain regions from LKO mice after PBS or VAL-1221 ICV treatment. Representative PAS staining images of the cortex, thalamus, cerebellum, and brain stem from LKO mice after ICV treatment with PBS or VAL-1221 shown at 40X magnification.

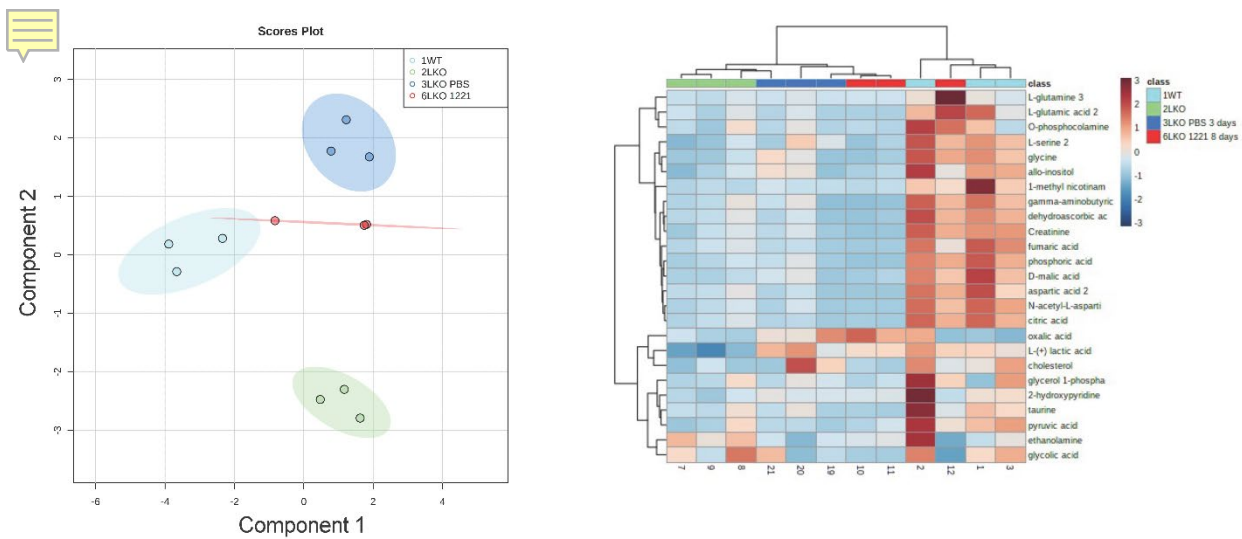


Figure 6: Correction of metabolic to WT in LKO mouse brains after ICV treatment with VAL-1221. PCA (A) and heatmap (B) of the metabolic profiles of WT mouse brains and LKO mouse brains treated via ICV with PBS or VAL-1221 determined using a GCMS approach.

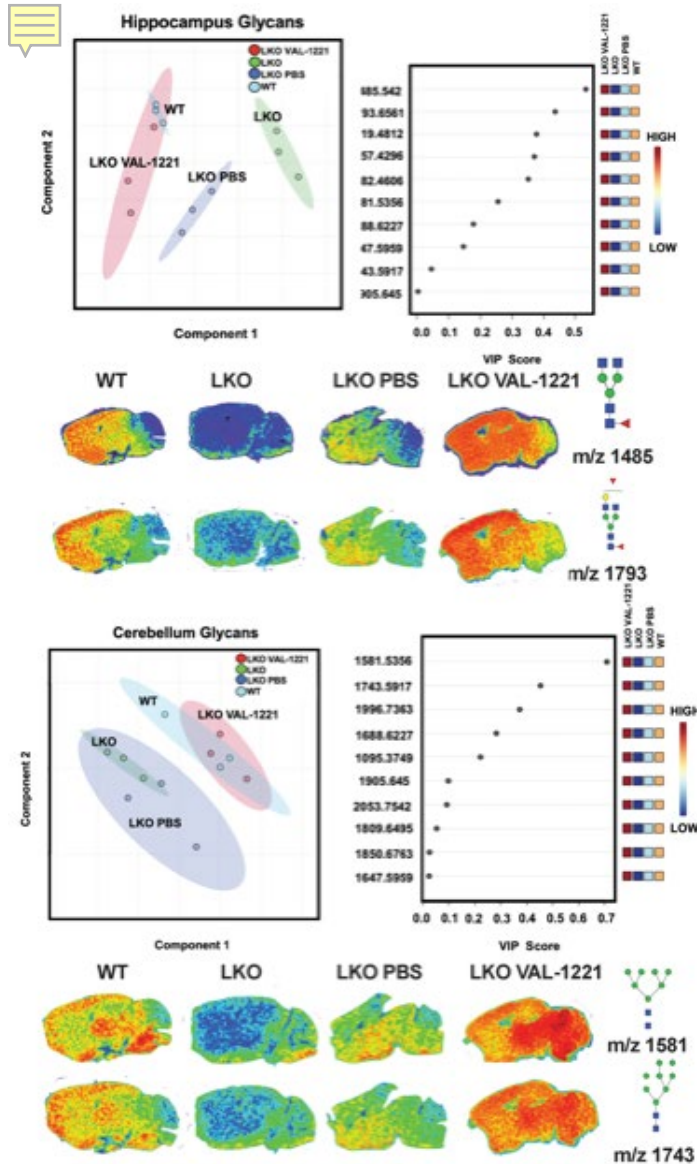
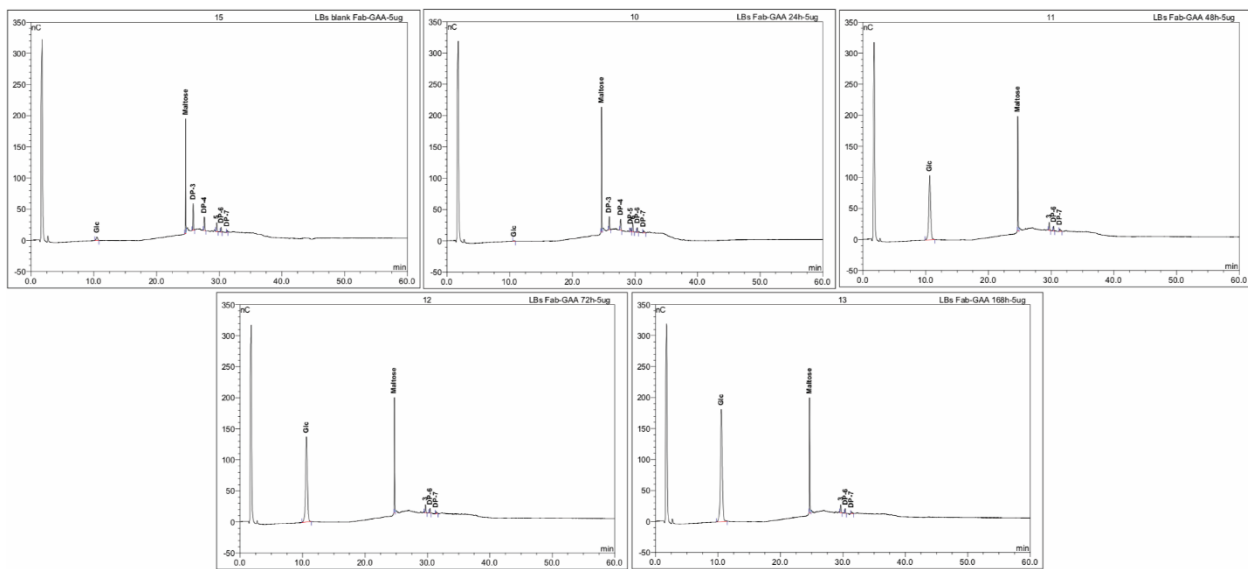


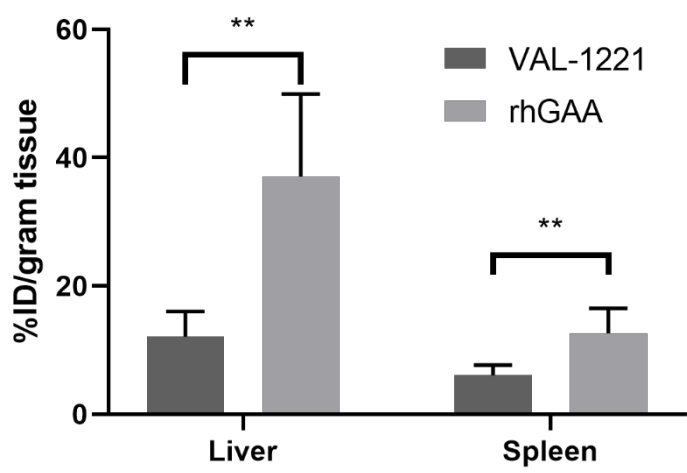
Figure 7: Correction of N-linked glycosylation profiles to WT in LKO mouse brains after ICV treatment with VAL-1221.

Cerebellum: sPLSDA (A) and VIP score (B) plots of the N-linked glycan profiles. Representative images (C) of the two most changed cell surface N-linked glycan distributions in WT mouse brains, LKO mouse brains, and LKO mouse brains ICV treated with VAL-1221 or PBS.

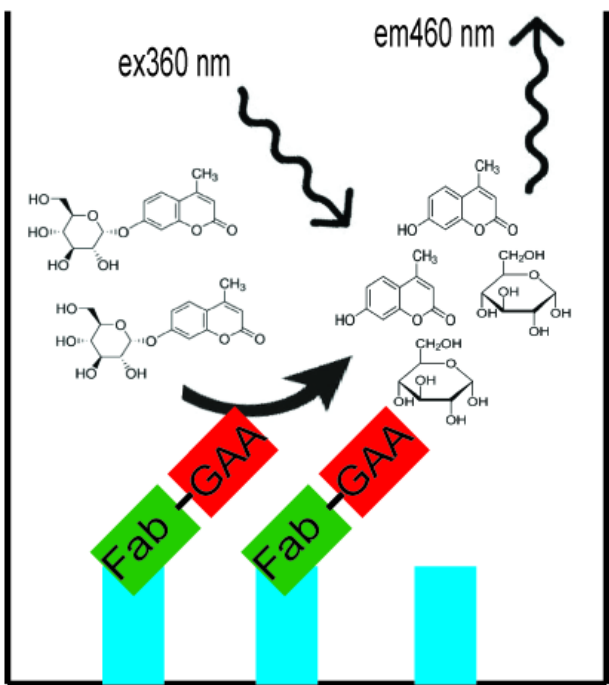
Hippocampus: sPLSDA (D) and VIP score (E) plots of the N-linked glycan profiles. Representative images (F) of the two most changed cell surface N-linked glycan distributions in WT mouse brains, LKO mouse brains, and LKO mouse brains ICV treated with VAL-1221 or PBS. Schematics of the specific glycans analyzed in these images follow X conventions.



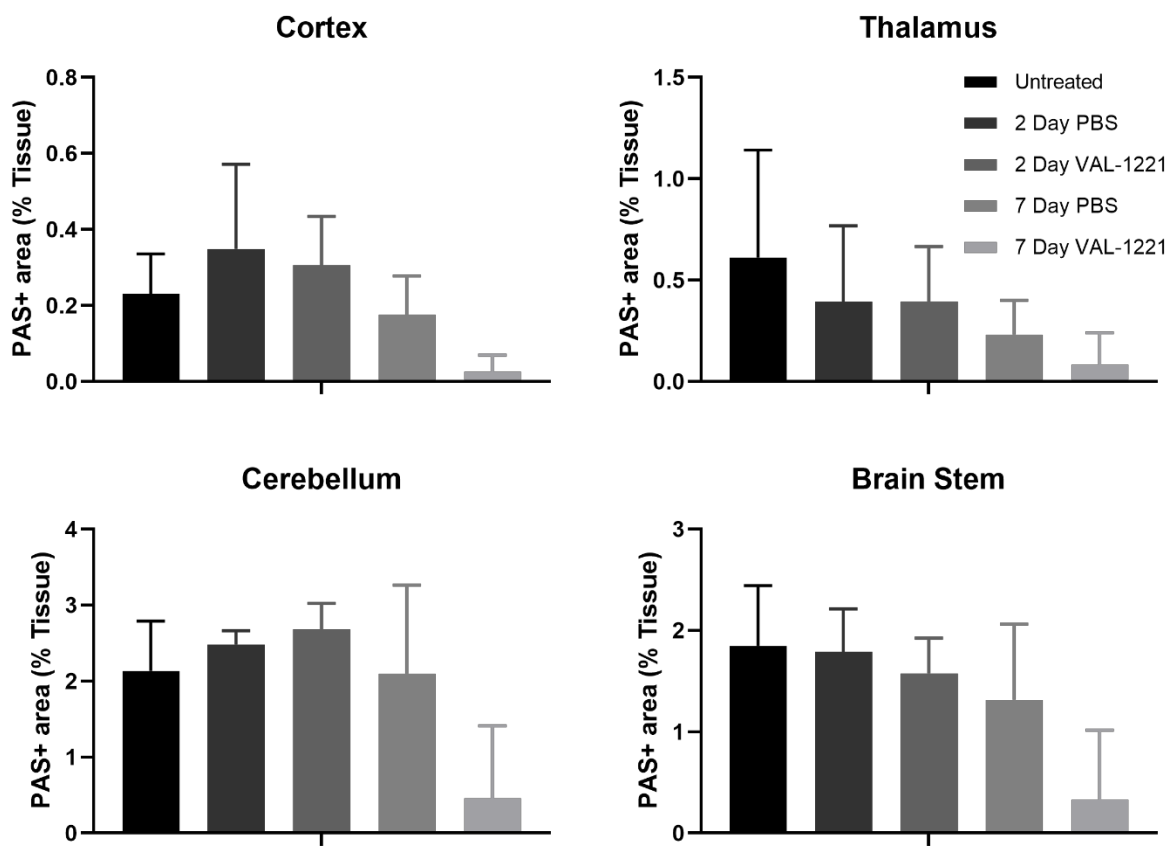
Supplemental Figure 1: HPAEC-PAD chromatograms of LKO mouse brain LB digestions with VAL-1221. Chromatograms showing the quantification of the different molecules released from LKO mouse brain LBs throughout an *in vitro* digestion with VAL-1221. Chromatograms are shown for all timepoints collected during the experiment (0, 24, 48, 72, and 168 hours).



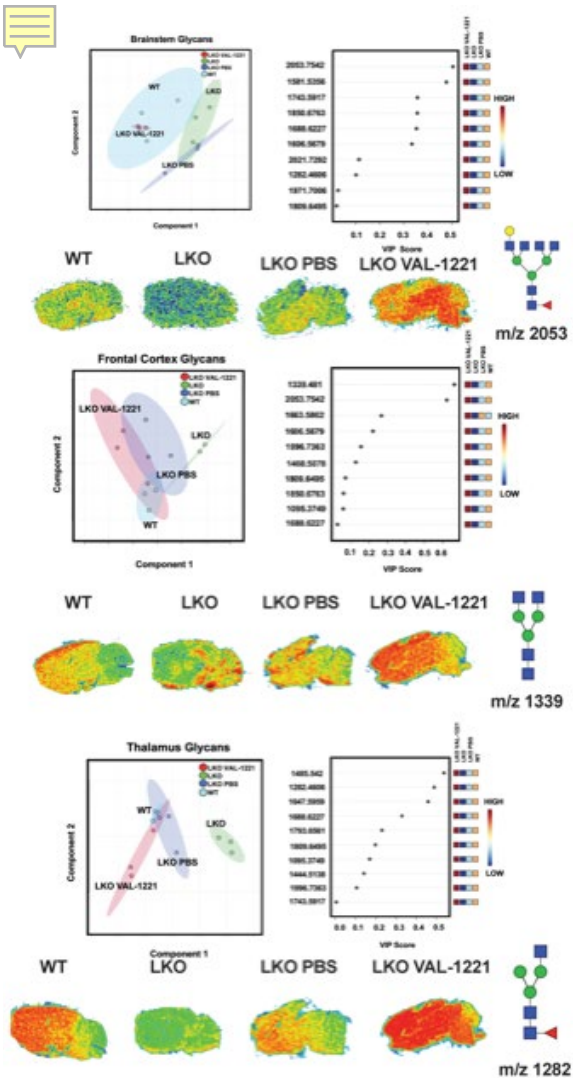
Supplemental Figure 2: Radiolabeled VAL-1221 biodistribution in WT mouse liver and spleen compared to radiolabeled rhGAA. Distribution of radiolabeled VAL-1221 or radiolabeled rhGAA in the liver and spleen in WT mice after TVI. Data presented as mean with SD error bars, ** p≤0.01.



Supplemental Figure 3: Schematic of the immunocapture enzyme activity assay for VAL-1221. VAL-1221 (red and green) is captured from tissue homogenate with an adsorbed anti-Fab antibody (blue). Then the abundance of VAL-1221 present is measured using the activity of the GAA segment of VAL-1221 against 4-MU-GP



Supplemental Figure 4: PAS+ area of different brain regions in LKO mice after ICV treatment with PBS or VAL-1221.
Graphs showing the PAS+ area from the cortex, thalamus, cerebellum, and brain stem, after ICV treatment with PBS or VAL-1221. Quantification was done using HALO image analysis software.



Supplemental Figure 5: Cell surface glycosylation correction in additional brain regions. Brain stem: sPLSDA (A) and VIP score (B) plots of the N-linked glycan profiles. Representative images (C) of the most changed cell surface N-linked glycan distribution in WT mouse brains, LKO mouse brains, and LKO mouse brains ICV treated with VAL-1221 or PBS. Thalamus: sPLSDA (D) and VIP score (E) plots of the N-linked glycan profiles. Representative images (F) of the most changed cell surface N-linked glycan distribution in WT mouse brains, LKO mouse brains, and LKO mouse brains ICV treated with VAL-1221 or PBS. Cortex: sPLSDA (G) and VIP score (H) plots of the N-linked glycan profiles. Representative images (I) of the most changed cell surface N-linked glycan distribution in WT mouse brains, LKO mouse brains, and LKO mouse brains ICV treated with VAL-1221 or PBS. Schematics of the specific glycans analyzed in these images follow X conventions.